The Birth and Evolution of Eastward-Propagating Modons

RICHARD P. MIED AND GLORIA J. LINDEMANN

Environmental Sciences Division, Naval Research Laboratory, Washington, DC 20375

(Manuscript received 15 July 1980, in final form 23 December 1981)

ABSTRACT

This paper addresses the tendency for an eastward-propagating modon to form from a mesoscale eddy which has an inclined vertical axis and different senses of rotation in the upper and deep oceans. This scenario, which has been observed in nature (McCartney *et al.*, 1978; Savchenko *et al.*, 1978), is modeled in a two-layer ocean by placing a cyclonic eddy in the upper ocean, and an anticyclonic eddy in the deep ocean; these two eddies have centers which are horizontally separated. Inferences about the tendency for modongenesis are made from analytical quasigeostrophic calculations and numerical primitive equation computations. Numerical experiments have been performed using radial velocity distributions $\propto r\exp(-r^2/2L^2)$ in each layer. These results not only corroborate the analytical early-time inferences but expand the parameter range for which modongenesis occurs.

If the upper ocean vortex is cyclonic and lies due north of the deep ocean anticyclonic gyre, modongenesis occurs when the vortex centers are separated by $\leqslant(1.5\text{–}2.0)L$. But if the deep ocean anticyclonic vortex is due north of the cyclonic one, modongenesis ensues when the separation is $\leqslant L/3$. The maximum separation at which modongenesis can occur varies continuously between these two extremes as the line of vortex centers is rotated from one configuration to the other. The modons so formed possess a barotropic core (Larichev and Reznik, 1976), and support superposed barotropic and baroclinic vortices (Stern, 1975; Flierl *et al.*, 1980); the propagation speeds, length scales and strengths of the resulting modons are examined in the light of these steady state theories.

1. Introduction

A great deal of effort has been devoted over the previous decade toward finding isolated mesoscale current systems which propagate with little or no change of form for long periods of time. One conspicuously successful line of research was initiated by Stern (1975) who used the term *modon* to designate an isolated barotropic current system consisting, in its simplest form, of a vortex pair with their centers at different latitudes but at the same longitude. Stern sought a steady, nonpropagating quasigeostrophic solution with the shapes and strengths of the two gyres adjusted so that the β-induced westward propagation tendency exactly canceled their mutual advection toward the east. He also noted that an axisymmetric vortex could be superimposed on his modon solution without altering the dynamics of the basic vortex pair. Flierl (1976) extended this concept to include a superposed baroclinic vortex in an ocean with continuous stratification. Larichev and Reznik (1976) showed that a barotropic modon could propagate toward the east as well as the west and indicated the conditions under which it could do so. More recently, Flierl *et al.* (1980) have unified the above theories to include modon propagation in a two-layer ocean. Although they discuss both eastward- and westward-propagating current systems, we shall concentrate in this study only upon one of the former varieties.

Of particular interest to the oceanographer is the question of viable mechanisms for the birth of modons. A significant first step has been made in this direction by Flierl (1976) who suggested that a pure baroclinic eddy would evolve in such a way as to spin up a barotropic modon. This idea was subsequently tested by McWilliams and Flierl (1979) using a two-layer quasigeostrophic numerical model and was indeed found to be a valid mechanism for modongenesis. One cannot ignore the potential geophysical importance of this process to ring evolution because of the wide range of relative strengths of the barotropic and first baroclinic modes found at different points along the Gulf Stream.

An equally interesting situation with respect to modon formation, however, may be that in which an eddy with a large first mode baroclinic component undergoes a tilting of its axis. We are interested in this configuration because a simple modal decomposition of such a configuration reveals two counter-rotating barotropic gyres, a flow *superficially* similar to the pure modon core of Larichev and Reznik. A clear example of this may be seen in the initial barotropic pressure distribution in Fig. 6 of this paper

which results when an upper ocean and deep ocean gyre do not share a common vertical axis (Figs. 4, 5).

And indeed, examples of tilted-axis eddies may be found in the literature. McCartney *et al.* (1978) have reported a survey of a large ring in the Northwestern Sargasso Sea in which the velocities above a depth of 2000 m are cyclonic, while those in the deep ocean are anticyclonic. The axis of zero current is skewed ~45 km laterally (estimated from their Fig. 15) over a 5 km depth along a northeast–southwest section. Aided by XBT (expendable bathythermograph), hydrographic, and current-meter data, Savchenko *et al.* (1978) construct a picture of an Antarctic Circumpolar Current eddy whose cyclonic upper-ocean flow lies somewhat to the east of the associated anticyclonic flow in the deep ocean. These observations are of eddies associated with different current systems, but are of special interest to this paper as they deal with tilted axis vortices having a deep-ocean current structure that rotates counter to that in the upper ocean. Motivated by these observations, we seek to address this question: under what circumstances could an initially baroclinic eddy, in which the axis is subsequently tilted, give rise to a readily identifiable eastward-propagating modon?

To answer this question, we employ analytical calculations for small time to yield results which may shed some light on the viability of different configurations of the tilted-axis scenario to give birth to a modon. The conclusions reached through these early-time calculations are supported by a number of numerical simulations using a primitive equation, two-layer model on a β-plane. We find that in some instances, a modon does not result, but that many situations do indeed lead to modongenesis.

Once generated, the modon changes as it propagates, and a subordinate goal of this work is to examine the state to which it evolves. In the latter portion of this paper then, we examine the relation of the physical quantities of the modon (sizes, shapes, and speeds) with respect to the steady state theory. We observe that in general, the vortex structure evolves *toward* a modon state, but is frequently observed to break up before equilibrating to the steady, eastward propagating ideal.

2. Preliminary considerations

The theory of the steady, eastward and westward propagating modon has been unified by Flierl *et al.* (1980), who have discovered an interesting number of variations of the basic modon concept. The variety of solutions available, however, and the concomitant difficulty in discerning qualitatively similar species, pose a potential problem in evaluating the experimental results. Led by appearance of the flows when decomposed into their barotropic and baroclinic modes, however, we choose for the simple modon model a barotropic core (the twin-gyre flow of Larichev and Reznik) with axisymmetric barotropic and baroclinic riders (the attached vortices of Flierl *et al.* (1980) which do not alter the dynamics of the barotropic core). We find that modon speeds and length scales are represented reasonably well. It is useful, for the purpose of this paper, to sketch the appropriate modon theory.

The equations for the barotropic (ψ_{BT}) and baroclinic (ψ_{BC}) modes in a two-layer system can be shown to admit time-independent first integrals with the assumption of steady zonal translation with speed U. Stern (1975) was the first to argue that such a flow must contain an interior region (radius $= (x^2 + y^2)^{1/2} = r \leq a$) and an exterior region ($r > a$). One class of first integrals may thus be written

$$\nabla^2\psi_{BT} + \begin{pmatrix}\kappa^2\\ \rho^2\end{pmatrix}\psi_{BT} = -\left[\beta + \begin{pmatrix}\kappa^2\\ \rho^2\end{pmatrix}U\right]y + \begin{pmatrix}\nu\\ 0\end{pmatrix}, \quad r \leq a,$$

$$\nabla^2\psi_{BC} + \left[\begin{pmatrix}\kappa^2\\ \rho^2\end{pmatrix} - R_d^{-2}\right]\psi_{BC} = \begin{pmatrix}\mu\\ 0\end{pmatrix}, \quad r \leq a,$$

where μ, ν, κ and ρ are constants and R_d is the internal radius of deformation. Solutions may be written in polar coordinates (r, θ) using Bessel and modified Bessel functions (J_0, J_1 and K_0, K_1, respectively) and circular trigonometric functions. The barotropic solution is given in terms of the constants C and D by

$$\psi_{BT} = \begin{cases} \left[\dfrac{a\beta}{\kappa^2}\dfrac{J_1(\kappa r)}{J_1(\kappa a)} - \dfrac{\beta + \kappa^2 U}{\kappa^2}r\right]\sin\theta + \nu/\kappa^2 + CJ_0(\kappa r), & r < a \\ -\dfrac{UaK_1[(\beta/U)^{1/2}r]}{K_1[(\beta/U)^{1/2}a]}\sin\theta + DK_0[(\beta/U)^{1/2}r], & r > a \end{cases} \tag{2.1}$$

Larichev and Reznik modon — Flierl, Larichev, McWilliams and Reznik barotropic rider

and the attached baroclinic vortex is written

$$\psi_{BC} = \begin{cases} AJ_0(\alpha r) + \mu/\alpha^2, & r < a \\ BK_0(\gamma r), & r > a \end{cases} \tag{2.2}$$

where A and B are constants and $\alpha = (\kappa^2 - R_d^{-2})^{1/2}$, $\gamma = (-\rho^2 + R_D^{-2})^{1/2}$, and $\rho^2 = -\beta/U$. The restriction that $[\psi]_{r=a} = [\partial\psi/\partial r]_{r=a} = 0$ (Lari-

chev and Reznik, 1976) has been used by Flierl *et al.* (1980) to obtain dispersion relations for both baroclinic and barotropic parts. To this, we also add the intuitively appealing assertion that $[\nabla^2\psi_{BC}]_{r=a} = 0$ with the expectation that smaller-scale processes will ultimately smooth vorticity discontinuities. These three conditions lead to a dispersion relation for the baroclinic rider

$$\begin{vmatrix} J_0(\alpha a) & -K_0(\gamma a) & 1/\alpha^2 \\ \alpha J_1(\alpha a) & -\gamma K_1(\gamma a) & 0 \\ \alpha^2 J_1'(\alpha a) & -\gamma^2 K_1'(\gamma a) & 0 \end{vmatrix} = 0,$$

or

$$\frac{J_1(\alpha a)}{(a\alpha)J_0(\alpha a)} + \frac{K_1(\gamma a)}{a\gamma K_0(\gamma a)} = 0, \quad (2.3)$$

which may be solved with the Larichev and Reznik dispersion relation

$$\frac{J_2(a\kappa)}{(a\kappa)J_1(a\kappa)} + \frac{K_2[(\beta/U)^{1/2}a]}{[(\beta/U)^{1/2}a]K_1[(\beta/U)^{1/2}a]} = 0. \quad (2.4)$$

These roots are displayed in Table 1, along with other relevant barotropic modon quantities. The dispersion relation showing $U/\beta R_d^2$ as a function of a/R_d is contained in Section 5. When the restriction that the vorticity of the barotropic rider be continuous at $r = a$ is also enforced, we obtain after similar manipulation

$$\frac{J_1(a\kappa)}{(a\kappa)J_0(a\kappa)} + \frac{K_1[(\beta/U)^{1/2}a]}{[(\beta/U)^{1/2}a]K_0[(\beta/U)^{1/2}a]} = 0. \quad (2.5)$$

Solutions to the system (2.4, 2.5) do not exist. Consequently, the barotropic flow, if it contains a rider, will not have a vorticity profile which is smooth; discontinuities in $\nabla^2\psi_{BT}$ must exist.

3. Early stages of modon formation

a. The governing equation

We model a baroclinic eddy with inclined axis by using an initially circular upper-ocean gyre and a circular deep-ocean gyre whose centers are displaced by a large horizontal distance. As we remarked in the introduction, the inclined axis eddy model described above can be seen to have a barotropic flow comprised of two counter-rotating gyres. Analysis of the experimental data indicates that this is indeed the case; and, moreover, axisymmetric barotropic and baroclinic riders appear to be present. Because the barotropic Larichev and Reznik core is the *sine qua non* for the riders, we are concerned with the conditions under which these equal strength barotropic gyres can form.

The quasigeostrophic barotropic equation for coupled barotropic/baroclinic flows is

$$\frac{\partial}{\partial t}\nabla^2\psi_{BT} + \frac{\partial\psi_{BT}}{\partial x} + M\frac{\partial(\psi_{BT}, \nabla^2\psi_{BT})}{\partial(x, y)} + M\frac{\partial(\psi_{BC}, \nabla^2\psi_{BC})}{\partial(x, y)} = 0, \quad (3.1)$$

where

ψ_{BT} = barotropic streamfunction,
ψ_{BC} = baroclinic streamfunction,
ψ_1 = upper layer streamfunction,
ψ_2 = deep ocean streamfunction,
x, y = east, north,
H_1 = upper ocean depth,

TABLE 1. The relationship of modon parameters when the condition $[\nabla^2\psi_{BC}]_{r=a} = 0$ is enforced upon the baroclinic rider solution of Flierl *et al.* (1980). $2l_{BT}$ is the distance between the extrema in barotropic core pressure, $\Delta\psi_{BT}$ is twice the maximum barotropic core pressure ($2 \times \max \psi_{BT}$), and R_d is the deformation radius.

a/R_d	$U/\beta R_d^2$	$a\kappa$	$\kappa U^{1/2}/\beta^{1/2}$	κl_{BT}	l_{BT}/R_d	$\Delta\psi_{BT}/\beta R_d^3$
3.375	0.002	5.069	0.067	2.005	1.3347	−6.345
3.325	0.009	4.994	0.143	2.006	1.3355	−6.405
3.275	0.021	4.919	0.220	2.008	1.3368	−6.512
3.225	0.040	4.845	0.300	2.011	1.3385	−6.667
3.175	0.065	4.772	0.382	2.015	1.341	−6.879
3.125	0.098	4.699	0.469	2.020	1.343	−7.154
3.075	0.140	4.630	0.562	2.026	1.346	−7.505
3.025	0.193	4.556	0.662	2.033	1.350	−7.948
2.975	0.262	4.486	0.772	2.041	1.354	−8.506
2.925	0.350	4.417	0.894	2.051	1.358	−9.212
2.875	0.465	4.350	1.032	2.062	1.363	−10.114
2.825	0.617	4.284	1.191	2.075	1.368	−11.290
2.775	0.823	4.219	1.380	2.090	1.374	−12.857
2.725	1.115	4.157	1.610	2.107	1.381	−15.026
2.675	1.547	4.095	1.904	2.128	1.390	−18.182
2.625	2.240	4.036	2.301	2.153	1.400	−23.125
2.575	3.491	3.979	2.887	2.183	1.413	−31.832
2.525	6.286	3.924	3.896	2.222	1.430	−50.799

H_2 = deep ocean depth,
$R = (H_2/H_1)^{1/2}$,
L = length scale of motion (radius from center of each vortex to its position of maximum current),
V_0 = characteristic velocity,
$M = V_0/\beta L^2$.

The upper and deep ocean flows may be written in terms of the normal modes (Flierl, 1978) as

$$\left.\begin{aligned}\psi_1 &= \psi_{BT} + R\psi_{BC}\\ \psi_2 &= \psi_{BT} - \frac{1}{R}\psi_{BC}\end{aligned}\right\}. \tag{3.2}$$

The streamfunctions, distances, and time have been nondimensionalized by V_0L, L and $(\beta L)^{-1}$, respectively.

Adem (1956) has used a power series in time to predict the translation tendency of barotropic atmospheric vortices, and McWilliams and Flierl (1979) have used it to great advantage in their work on mixed barotropic/baroclinic vortices. We may use this technique to make similar predictions regarding the more complicated twin-vortex configurations in the present work. For small times [dimensional time $\ll (\beta L)^{-1}$], we write

$$\psi_{BT} \sim \psi_{T0} + \psi_{T1}t + \psi_{T2}t^2 + \cdots,$$

$$\psi_{BC} \sim \psi_{C0} + \psi_{C1}t + \psi_{C2}t^2 + \cdots,$$

where ψ_{T0} and ψ_{C0} are the barotropic and baroclinic vortex configurations at $t = 0$. To $O(t^0)$ then, we see that

$$\nabla^2\psi_{T1} = -\left\{\frac{\partial}{\partial x}\psi_{T0} + M\left[\frac{\partial(\psi_{T0}, \nabla^2\psi_{T0})}{\partial(x, y)} + \frac{\partial(\psi_{C0}, \nabla^2\psi_{C0})}{\partial(x, y)}\right]\right\}. \tag{3.3}$$

If initially,

$$\left.\begin{aligned}\psi_1 &= A\exp[-(x - x_0)^2 - (y - y_0)^2]/2 = Ae_-\\ \psi_2 &= B\exp[-(x + x_0)^2 - (y + y_0)^2]/2 = Be_+\end{aligned}\right\}, \tag{3.4}$$

then (3.2) yields

$$\psi_{T0} = \frac{Ae_- + BR^2e_+}{1 + R^2} \quad \text{and}$$

$$\psi_{C0} = \frac{R(Ae_- - Be_+)}{1 + R^2}. \tag{3.5a,b}$$

Substitution of (3.5a,b) into (3.3) reveals that the first correction to the initial conditions is governed by

$$\nabla^2\psi_{T1} = -\frac{\partial}{\partial x}\psi_{T0} - M\frac{\partial(\psi_{T0}, \nabla^2\psi_{T0})}{\partial(x, y)} - M\frac{\partial(\psi_{C0}, \nabla^2\psi_{C0})}{\partial(x, y)}$$

$$= \frac{+A(x - x_0)e_- + B(x + x_0)R^2e_+}{1 + R^2} + \frac{16ABR^2M}{(1 + R^2)^2}(xx_0 + yy_0)(x_0y - xy_0)e^{-r^2}e^{-r_0^2}, \tag{3.6}$$

where $r^2 = x^2 + y^2$ and $r_0^2 = x_0^2 + y_0^2$. The first term on the right-hand side is simply the linear propagation/dispersion of the vortex pair. The second term represents the advection of one vortex by the barotropic and baroclinic currents in the other. Because each eddy is circular, the *self* advection terms [of the form $\partial(e_+, \nabla^2e_+)/\partial(x, y)$] vanish, but one vortex may influence the other. Moreover, the strength of this interaction is dependent upon the product of their individual strengths (A, B) and decreases rapidly as their separation distance ($\sim 2r_0$) increases.

b. The propagation/dispersion solution

We note that because the Laplacian is invariant under the transformation

$$x \pm x_0 \rightarrow x,$$

$$y \pm y_0 \rightarrow y,$$

the formidable propagation/dispersion part of (3.6) for the vortex pair may be reduced to a simple canonical equation. Thus,

$$\nabla^2\phi = Cxe^{-r^2/2},$$

where

$$C = \begin{cases} A/(1 + R^2) & \text{for the northern vortex} \\ BR^2/(1 + R^2) & \text{for the southern vortex}. \end{cases}$$

We define the Fourier transform as

$$\hat{\phi}(\kappa, l) = \int_{-\infty}^{+\infty}\int_{-\infty}^{+\infty}\phi(x, y)e^{i(kx+ly)}dxdy.$$

Taking advantage of symmetry properties of the integrand, we may write [Erdelyi (1954; Section 2.4(19), 1.4(11)]

$$\hat{\phi} = \frac{-2\pi Cike^{-(k^2+l^2)/2}}{k^2 + l^2},$$

and then

$$\phi = \frac{C}{(2\pi)^2}\int_{-\infty}^{+\infty}\int_{-\infty}^{+\infty}\hat{\phi}(k, l)e^{-i(kx+ly)}dkdl.$$

Now we define Φ such that $\phi \equiv \partial\Phi/\partial x$; thus,

$$\Phi = \frac{C}{2\pi}\int_{-\infty}^{+\infty}\int_{-\infty}^{+\infty}\frac{e^{-(k^2+l^2)/2}}{k^2 + l^2}e^{-i(kx+ly)}dkdl.$$

In polar coordinates,

$$\Phi = 2\pi C \int_0^\infty \int_0^{2\pi} \frac{e^{-\rho^2/2}}{\rho} e^{-i\rho r\cos\alpha} d\rho d\alpha,$$

where $\cos\alpha = (k, l)\cdot(x, y)/|\rho|\cdot|r|$ and $\rho = (k^2 + l^2)^{1/2}$, so that

$$\Phi = 2\pi C \int_0^\infty \frac{d\rho}{\rho} e^{-\rho^2/2} \int_0^{2\pi} e^{-i\rho r\cos\alpha} d\alpha$$

$$= C \int_0^\infty \frac{e^{-\rho^2/2}}{\rho} J_0(\rho r) d\rho$$

(by Abromowitz and Stegun, 1965; Section 9.1.21). Then

$$\phi = \partial\Phi/\partial x = -C \int_0^\infty \frac{x}{r} e^{-\rho^2/2} J_1(\rho r) d\rho$$

$$= -\frac{x\sqrt{2\pi}}{2r} C e^{-r^2/4} I_{1/2}(r^2/4),$$

where I_j is a modified Bessel function. Therefore,

$$\phi(x, y) = \frac{Cx}{r^2}(e^{-r^2/2} - 1),$$

which gives the propagation/dispersion behavior of ψ_{T1} for a single vortex.

c. *The mutual advection solution*

We may solve the advection portion of (3.6) in a similar fashion. It is convenient to rotate the coordinate system so that the vortex centers lie on the x' axis of the new system (x', y'). Thus,

$$x' = x\cos\theta + y\sin\theta = \frac{1}{r_0}(xx_0 + yy_0),$$

$$y' = -x\sin\theta + y\cos\theta = \frac{1}{r_0}(yx_0 - xy_0),$$

where $(x_0, y_0)/r_0 = (\cos\theta, \sin\theta)$ and $r_0^2 = x_0^2 + y_0^2$. Dropping primes and expressing the advection part in the rotated frame, we see that our canonical equation becomes

$$\nabla^2\phi = cxye^{-r^2},$$

where

$$c = +\frac{16ABR^2M}{(1 + R^2)^2} r_0^2 e^{-r_0^2}.$$

We obtain $\hat{\phi}$ much as before, and invert the transform to obtain ϕ:

$$\phi(x, y) = \frac{1}{(2\pi)^2} \int_{-\infty}^{+\infty} \int_{-\infty}^{+\infty} \frac{\pi klc}{4(k^2 + l^2)} \times e^{-k^2/4} e^{-l^2/4} e^{-i(kx+ly)} dk dl.$$

Again, it is convenient to define

$$\Phi(x, y) = -\frac{c}{16\pi} \int_{-\infty}^{+\infty} \int_{-\infty}^{+\infty} \frac{(e^{-k^2/4})e^{-l^2/4}}{k^2 + l^2} e^{-i(kx+ly)} dk dl,$$

so that $\phi = \partial^2\Phi/\partial x\partial y$. We may express this in polar coordinates:

$$\Phi = -\frac{c}{16\pi} \int_0^\infty \int_0^{2\pi} \frac{e^{-\rho^2/4}}{\rho} e^{-i\rho r\cos\alpha} d\rho d\alpha$$

$$= -\frac{c}{8} \int_0^\infty \frac{e^{-\rho^2/4} J_0(\rho r)}{\rho} d\rho.$$

Then

$$\partial\Phi/\partial x = +\frac{cx}{8r} \int_0^\infty e^{-\rho^2/4} J_1(\rho r) d\rho = \frac{x}{8r} e^{-r^2/2} I_{1/2}(r^2/2)$$

so that

$$\phi = c\left[\frac{xy}{4r^2} e^{-r^2} + \frac{xy}{4r^4}(e^{-r^2} - 1)\right].$$

The solution of (3.6) is then given by

$$\psi_{T1} = \frac{A}{1 + R^2} \frac{(x - x_0)}{[(x - x_0)^2 + (y - y_0)^2]} \times \{e^{-[(x-x_0)^2+(y-y_0)^2]/2} - 1\} + \frac{BR^2}{1 + R^2} \frac{(x + x_0)}{[(x + x_0)^2 + (y + y_0)^2]} \times \{e^{-[(x+x_0)^2+(y+y_0)^2]/2} - 1\} + \frac{4ABR^2M}{(1 + R^2)^2} \frac{(xx_0 + yy_0)(x_0y - xy_0)}{(x^2 + y^2)} e^{-(x_0^2+y_0^2)} \times \left\{e^{-(x^2+y^2)} + \frac{e^{-(x^2+y^2)} - 1}{x^2 + y^2}\right\}. \quad (3.7)$$

The positions of x_0 and y_0 may be specified to give not only an initial separation of the two vortices [defined to be $2r_0 = 2(x_0^2 + y_0^2)^{1/2}$], but the angle of inclination (α) of their centers with respect to north. These two parameters, along with vortex strengths (A, B) and ratio of layer heights $R\ (=H_2/H_1)^{1/2}$ have a bearing upon whether a modon will be formed from a baroclinic vortex with an inclined axis. Although all parameters are of interest, we fix $R^2 = 4000$ m/1000 m = 4 for this study and vary α, and the separation distance $2r_0$. The relative magnitudes of these parameters then determine whether the propagation/dispersion terms (first two in 3.7) will dominate the mutual advection term (last one on right), at least initially. A net eastward motion prevents the immediate dispersal of the energy toward the west, and allows the higher-order terms further opportunity for modongenesis.

d. *Examples of early-time behavior*

Using (3.7), we may now predict the vortex motion for small time. An approximation to the barotropic

TABLE 2. Synopsis of experiments in which cyclonic speeds are positive, and anticyclonic ones negative. The separation distance is defined as $2(x_0^2 + y_0^2)^{1/2}$. The angle of inclination α is zero when the center of the upper ocean vortex is due north of that of the deep ocean vortex. α increases in a counterclockwise fashion. Experiments 38–43 are of 100 days duration; all others last 150 days.

Experiment	U_1 (cm s^{-1})	U_2 (cm s^{-1})	α	Separation (km)	modon?
12	100	−25	—	0	yes
21	−100	25	—	0	yes
22	100	−30	0°	80	yes
23	100	−30	0°	160	no
25	100	−25	180	80	no
26	100	−25	+90°	80	no
27	100	−25	+45	84.9	yes
38	100	−25	−90	40	yes
39	100	−25	−90	20	yes
40	100	−25	−45	56.6	yes
41	100	−25	+135	56.6	no
42	100	−25	180	20	yes
43	100	−25	−45	141.4	no

stream function ($\psi_T \approx \psi_{T0} + \psi_{T1}t$) may be constructed and superimposed upon that for $t = 0.0$. If we choose A and B to correspond to the fixed upper and deep ocean velocities in this work (100 and −25 cm s^{-1}; see Table 2), then α and the separation distance may be varied to examine their effect upon modongenesis.

The positions of the gyre centers for $t > 0$ relative to their locations at $t = 0$ will indicate an initial eastward (modongenesis) or westward motion (vortex separation). However, these results must be taken as suggestive of, rather than indicative of actual vortex motion. There are two reasons for this. The first is that although the Rossby number is not large[1], the numerical experiments frequently exhibit interface elevations of ~350 m. As this is a significant fraction of the rest height $H_1 = 1000$ m, we expect that inferences from quasigeostrophic calculations may differ in detail from those of the primitive equation numerical model. The second reason is that the early-time model really only addresses initial tendencies of vortex pair evolution. Terms of higher order in t are frequently important; in fact, we shall document a case in Section 4.b (EXP 42) which is quite interesting. The analytical calculations would not suggest modongenesis, but the numerical experiments clearly show that a modon does indeed result. In spite of these two points, we feel that these analytical calculations can be instructive, particularly when used with the numerical experiments.

In Fig. 1, we show a matrix of calculations in which contours of ψ_T at $t = 0.5$ (4.83 days for this study; see Section 4.a) and ψ_T at $t = 0.0$ are shown as solid and dashed lines respectively. The nondimensionalized separation distance $2r_0 = 2(x_0^2 + y_0^2)^{1/2}$ and the inclination angle α are varied, and the results differ significantly, one from another. For $\alpha = 0.0°$, there is virtually no advection tendency when $2r_0 = 0.5$, but a significant eastward propagation tendency exists for $2r_0 = 1.5$. When $2r_0$ is increased to 3.0, this effect again becomes negligible. For distances greater than this, the mutual eastward advection term in 3.7 is incapable of overcoming the westward-directed propagation/dispersion effect. This change of behavior with increasing r_0 occurs because the mutual advection part of the stream function is a strong function of r_0, behaving as $r_0^2 e^{-r_0^2}$.

Increasing α from zero is almost as effective as large vortex separation in ameliorating the mutual advection tendency. Although the mutual advection tendency is independent of α, its direction is perpendicular to the line of vortex centers. Thus, as $|\alpha| \uparrow 90°$, less of this advection is directed eastward to oppose the beta-caused propagation/dispersion to the west. Vortex separation thus ensues. For constant r_0, it is seen (Fig. 1) that as α is increased, a point is reached where modongenesis is impossible. The values of α and r_0 thus work in concert to cause either modongenesis or vortex dispersion. A necessary condition for a modon to form is that $2r_0 \leqslant 1.5$ when $\alpha = 0.0$; this requisite value of $2r_0$ decreases to 0.0 (for this linear analysis) as $|\alpha| \uparrow 90.0°$.

These inferences are supported fairly well by the results of the numerical experiments. The information contained in Table 2 is presented more graphically in Fig. 2. The deep ocean vortex is located at the origin of the polar plot, and the dot and experiment number are located at the center of the point $(2r_0, \alpha)$. The region inside the closed curve marked with cross hatching is the region of parameter space where modongenesis occurs; no modons are formed in the exterior region. The two areas are separated by a cross-hatched line because this boundary is known only approximately, having been drawn in accordance with the behavior of the numerical experiments. Nevertheless, we do observe that when $\alpha = 0.0$, the boundary lies at $2r_0 \simeq 2.0$. As $|\alpha| \uparrow 90°$, the boundary occurs at smaller separations ($2r_0$). We expect that for $2r_0 \ll 1$, modongenesis (for any α) is governed by the nonlinear mechanism of McWilliams and Flierl (1979), and this accounts for the observed modon formation even when $|\alpha| = 90°$. EXP 42 is an interesting variant of this process that will be discussed in Section 4.b.

4. Experimental simulations

In Section 3, we investigated the initial tendencies of the quasigeostrophic barotropic flow for paired vortices as the relative positions of their centers are varied. While these calculations give an indication

[1] The Rossby number $V_0/f_0L = 10^2$ cm s^{-1}/(7.3 × 10^{-5} s^{-1}) (6 × 10^6 cm) = 0.23.

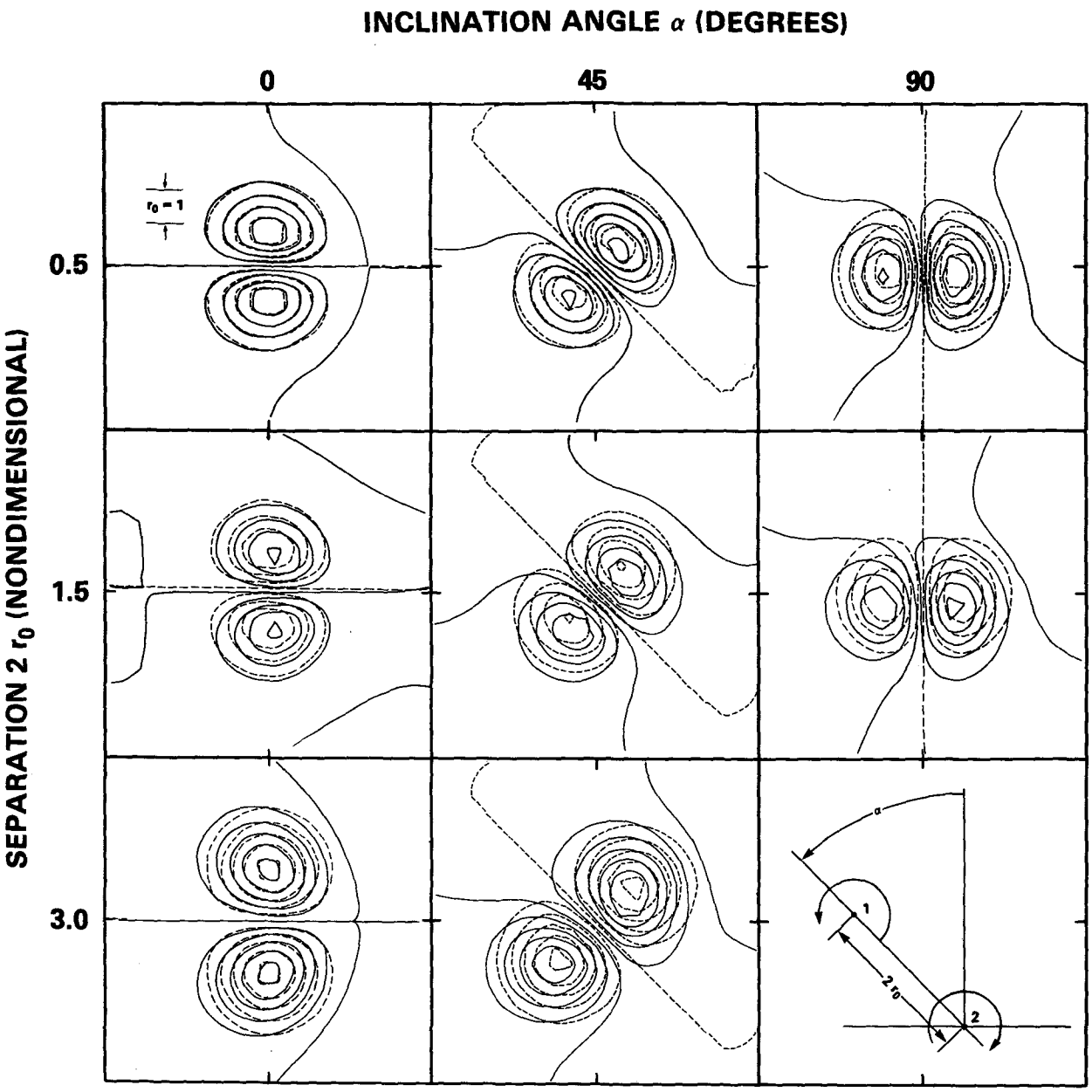

FIG. 1. Contours of constant $\psi_{T0} + \psi_{T1}t$ (solid lines) and ψ_{T0} (dashed lines) for $t = 0.5$ (4.83 days in this work). The nondimensional distance $r_0 = 1$ (60 km here) is shown in the top left and the separation distance ($2r_0$) and inclination angle α are defined. $\beta = 2 \times 10^{-13}$ cm^{-1} s^{-1}, $V_0 = 100$ cm s^{-1}, so $A = -e^{1/2}$, $B = 0.25e^{1/2}$, and $M = 13.89$. Contour intervals are 0.02 for the case $2r_0 = 0.5$, and 0.06 for the cases $2r_0 = 1.5$, 3.0.

of what will happen in the short-term evolution of the flow, they are incapable of giving details for much longer times. To obtain this information, we employ numerical simulations.

a. Details of the model

For these simulations, we employ a depth-averaged primitive equation two-layer beta-plane model with a flat bottom and rigid lid (Holland and Lin, 1975). The initial flow and interface displacement are presumed to be geostrophically balanced at $t = 0$, so that the vortex evolution is thus an initial value problem for which integration is performed in a 1000 km square box. As the use of this model has been thoroughly documented in a similar study (Mied and Lindemann, 1979), no details are given here. It is important to point out that the proximity of the walls does contaminate the observed pressures as well as the measured speeds of the resulting mo-

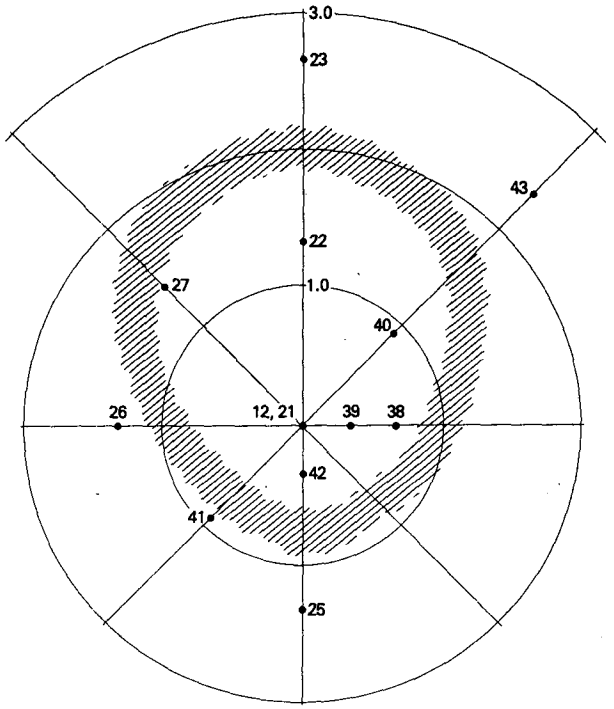

FIG. 2. The modongenesis parameter range in the $(2r_0, \alpha)$ polar plane is contained inside the cross-hatched loop. Vortex separation occurs elsewhere. The position of each experiment and its number is given.

dons. From Mied and Lindemann (1979), we do know that the pressure in the center of an evolving eddy in these experiments is unaffected by wall-reflected waves for the first 25 days. The experiments for this paper are of 100–150 days duration however, because we feel that the conclusions reached are qualitatively unaltered by the presence or absence of lateral boundaries. In fact our results indicate that for $t \geq 25$ days the pressures outside the eddies at a fixed point in the box show fluctuations which are at most 15% of the central eddy pressures with which we are concerned.

The parameters which are considered fixed in this study are

H_1 = upper ocean depth = 1000 m
H_2 = deep ocean depth = 4000 m
g' = reduced gravity = 2 cm s^{-2}
$f_0 = 7.3 \times 10^{-5}$ s^{-1}
$\beta = 2 \times 10^{-13}$ cm^{-1} s^{-1}

$$R_d = \frac{1}{f_0}\left(\frac{g'H_1H_2}{H_1 + H_2}\right)^{1/2} = 54.8 \text{ km}$$

L = 60 km.

The coefficient of lateral viscosity is fixed to be 2.5×10^5 cm^2 s^{-1} and $\nabla^2\mathbf{u}$ damping is employed. When pressures are quoted in the results, their units are expressed as m^2 s^{-2} because the actual pressures have been divided by a Boussinesq density.

We remind the reader that the numerical calculations employ a rigid-lid primitive-equation model, but that the analytical work of Sections 2 and 3 use the rigid lid quasigeostrophic equations. Both of these rigid-lid formulations exclude the rapid westward-propagating barotropic modons of Larichev and Reznik (1976). Moreover, the differences in the two types of model equations used are probably responsible for some of the slight differences noted between the numerical and analytical results.

b. The numerical experiments

Our objective is to obtain information about the long term (time $\geq 1/\beta L$ = 9.65 days) evolution of the eddy configurations shown in Table 2. For the sake of limiting the simulations to a manageable number, we have kept the upper and deep ocean velocities to be 100 and 25 cm s^{-1} (occasionally 30), respectively. It is useful to group these experiments into classes and discuss them in the light of the results of Section 3. Because experiments 12 and 21 spin up modons by a slightly different mechanism (McWilliams and Flierl, 1979) than that embodied in the physics described in Section 3; they will not be dis-

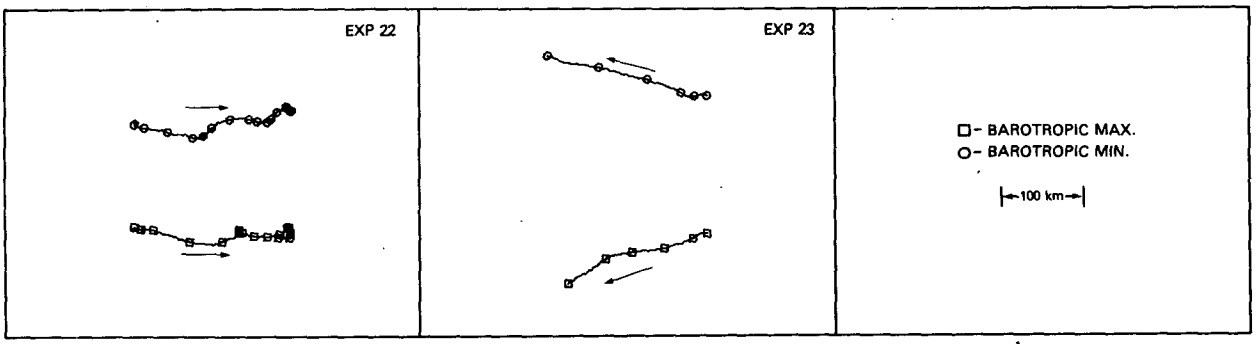

FIG. 3. The trajectories of the barotropic pressure extrema for EXP 22 (150 days) and EXP 23 (50 days). Symbols are placed at day 0 and on every succeeding tenth day.

cussed here, although the data from them is examined in Section 5. All of the remaining experiments, however, vary either the angle of inclination (α) of the eddy centers with respect to north, or the horizontal separation distance between the upper ocean and the lower ocean vortices.

The case $\alpha = 0.0°$ is represented by EXPs 22 and 23, which have gyre separation distances of 80 and 160 km ($2r_0 = 1.33$ and 2.67), respectively. From Section 3, we expect that in this $\alpha = 0.0°$ case only the lesser of these two separation distances should result in modongenesis, and the numerical experiments exhibit the expected behavior. In Fig. 3, we show the trajectories of the two barotropic pressure extrema for these two experiments and the differences are striking. EXP 22 shows a predominantly eastward propagation of the vortex pair. EXP 23 exhibits markedly different behavior. In this experiment, the vortices separate, with the cyclonic one propagating northwest and the anticyclonic one traveling southwest as expected. It is illuminating to examine the details of EXPs 22 and 23 because many of them are shared by other modongenesis experiments. In later discussing these others, only observations peculiar to those experiments need then be displayed. Furthermore, because the barotropic part of the flow is so crucial to the modon's existence, we shall be able to concentrate exclusively on this description below.

In Figs. 4, 5 the evolution of the flows in the upper and lower ocean for EXP 22 are shown. The distortion of the constant pressure lines (equivalent to streamlines in the quasigeostrophic approximation) is apparent in the deep ocean. More informative, however, are the barotropic pressure contours P_{BT} for the same times (Fig. 6). In Section 3, we noted a

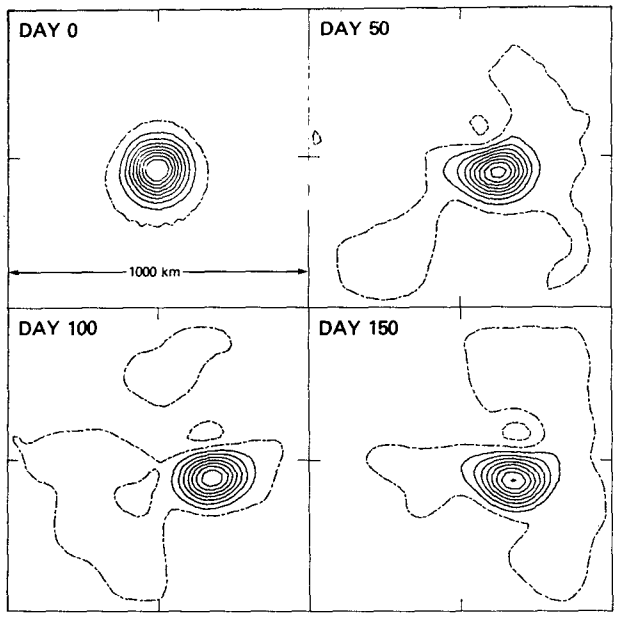

FIG. 5. Deep ocean pressure (P_2) for days 0, 50, 100, and 150 for EXP 22. Contour code as in Fig. 4; contour interval = 0.2 m^2 s^{-2}. The computational domain is 1000 km square.

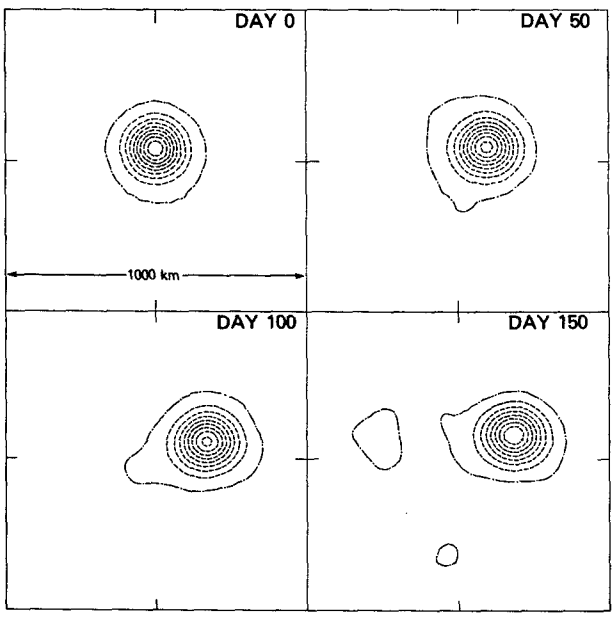

FIG. 4. Upper ocean pressure (P_1) for days 0, 50, 100, 150 for EXP 22. The upper ocean gyre is 80 km north of that in the deep ocean (shown in Fig. 6). Contour code: short-dashed line, $P_1 < 0$; long-dashed line, $P_1 = 0$; and solid line, $P_1 > 0$. Contour interval = 0.9 m^2 s^{-2}. The numerical simulation box is 1000 km square.

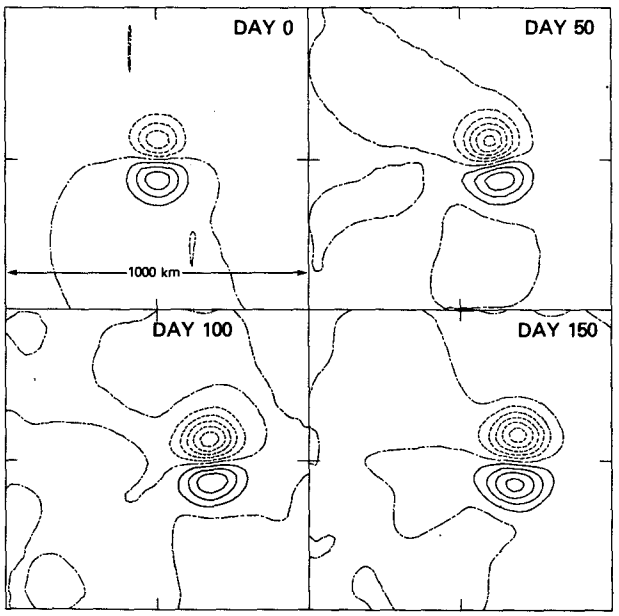

FIG. 6. Barotropic pressure (P_{BT}) for days 0, 50, 100 and 150 for EXP 22. Contour code as in Fig. 4; contour interval = 0.3 m^2 s^{-2}. The box is 1000 km square.

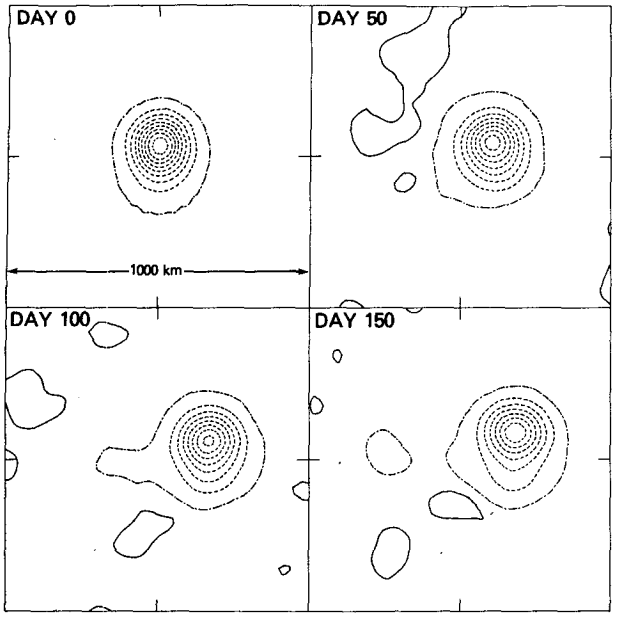

FIG. 7. Baroclinic pressure (P_{BC}) for days 0, 50, 100, and 150 for EXP 22. Contour code as in Fig. 4; contour interval = 0.4 m^2 s^{-2}. The only positive contour level = 0.12 m^2 s^{-2}. The box is 1000 km square.

strong tendency toward modongenesis in this case and this is observed in this figure. On day 0, we see a rather weak twin-vortex structure which becomes intensified considerably by day 50 and propagates east. The slight counter-clockwise rotation of the line of vortex centers at this time may be viewed alternately as a higher-order effect (in the t expansion) or as the advection of the barotropic modon core by the cyclonic barotropic rider, which grows in intensity for the first few tens of days (discussed in Section 5). Evidence of this low pressure vortex may be seen in Fig. 6 from days 50–150 because its presence enhances the low pressure already present in the northern cyclonic eddy and offsets that in the southern anticyclonic one. Thus, the northern gyre is more intense than the southern one.

The baroclinic flow (Fig. 7) never attains the circular symmetry dictated by the equilibrium theory (Section 2). Moreover, the southern portion of the flow has become markedly distorted by day 150 because the barotropic modon core is dispersing (discussed in Section 5). The related subtle question of when the behavior of any vortex pair *is* that of a modon is dealt with in Section 5 of this paper.

In rather sharp contrast to the behavior of EXP 22, the initial eddy configuration in EXP 23 does not exhibit any tendency to evolve into a mixed barotropic/baroclinic modon. The centers of the eddies in EXP 23 are initially separated by 160 km as opposed to the 80 km separation used in EXP 22. As discussed in Section 3, this is simply too great a distance for the mutual advective effect to offset the westward β-tendency, and the upper- and deep-ocean gyres propagate essentially independently of one another. The contours of constant barotropic pressure at day 50 are shown in Fig. 8, and the latitudinal compression characteristic of a barotropic modon is absent. Moreover, we note that each vortex possesses a configuration at least qualitatively consistent with the temporal evolution of a vortex of the appropriate sign (Mied and Lindemann, 1979). In particular, the characteristic dispersing wake can be seen behind each eddy. And finally, the trajectories of the northern (cyclonic) and southern (anticyclonic) vortices (Fig. 3) are consistent with our expectations based upon simple arguments invoking conservation of potential vorticity.

The cases in which $|\alpha| \neq 0.0°$ are interesting because of the richness of the interaction which can occur between the vortices as the pair evolves together. For $|\alpha| = 45.0°$, we have performed EXPs 40, 27, and 43 (Table 2) which correspond to $2r_0$ = 0.94, 1.41 and 2.36, respectively. From Fig. 1, we might predict that EXP 40 would probably result in a modon, 43 definitely would not, while 27 may lead to modongenesis. In fact, inferences from the small time calculations of Section 3 are surprisingly accurate in this case. In Fig. 9, we show the trajectories of the barotropic pressure maxima and minima for these three experiments, and the results are closely related to our predictions. The $2r_0 = 0.94$ case (EXP 40) is initiated with gyre centers located so that $\alpha = -45.0°$. The northern barotropic part propagates initially westward, but is soon advected eastward, and the southern eddy moves even more rapidly east-

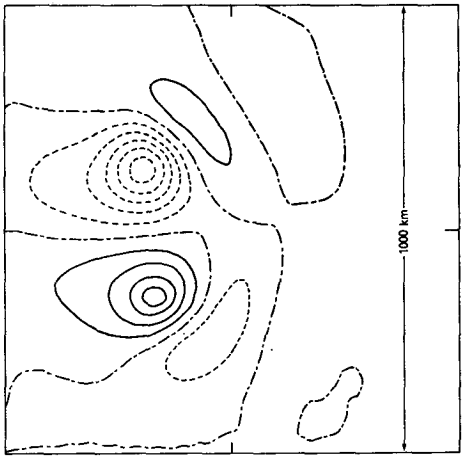

FIG. 8. Map of P_{BT} on day 50 for EXP 23. Contour code as in Fig. 4. Contour interval = 0.3 m^2 s^{-2}. Largest-valued positive contour level = 1.1 m^2 s^{-2}. The box is 1000 km square.

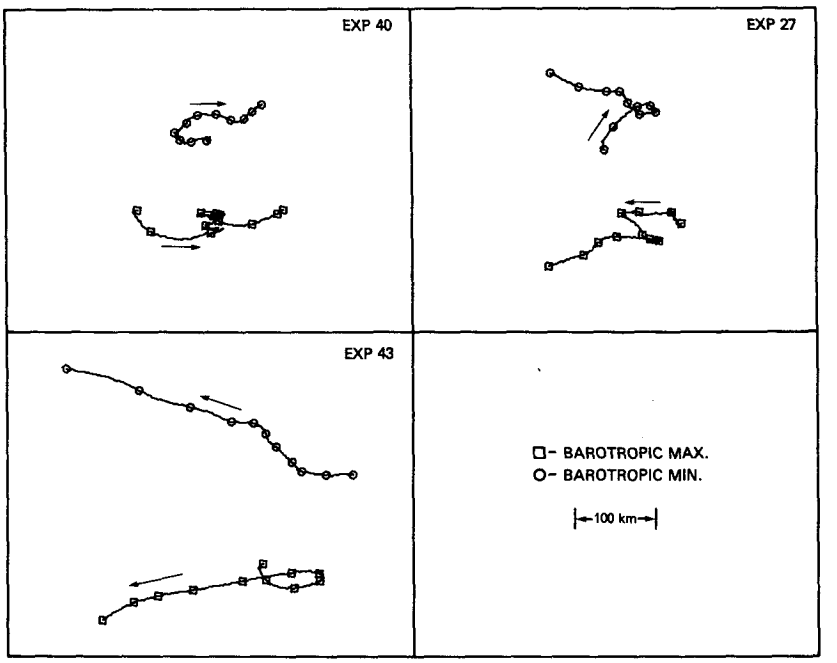

FIG. 9. Trajectories of barotropic pressure extrema for EXPs 40, 27, 43 (in order of increasing r_0) which are initialized with $|\alpha| = 45.0°$. Symbols are placed at the locations at day 0 and for every succeeding tenth day.

ward from the start. After less than twenty days however, it has overtaken the anticyclonic northern gyre and the pair then oscillate briefly about the $\alpha = 0.0$ configuration as they evolve together. This apparently complicated trajectory belies the simplicity of the motion which emerges clearly when pressure contours are viewed. We exhibit these in Fig. 10 and the oscillation of the line of vortex centers following the initial eastward overshoot of the southern vortex is seen to slowly decrease in amplitude, but to persist at least until day 100.

Our ambivalent feelings about the prospects for modongenesis in EXP 27 ($\alpha = +45.0°$) are confirmed by the trajectories of the barotropic extrema (Fig. 9). We see that shortly after initiation, the line of centers between the barotropic vortices rotates clockwise; by day 20, the vortex centers are located at a common longitude. This rotation in fact continues up to day 40, but the physical appearance of the vortex pair (Fig. 11) at that time does not appear to be that of a modon. In the next section, we shall show that the vortex pair is in the modon state up to about day 35. That is, the attached baroclinic vortex propagates to the east and the speeds, intensity, and dimensions of the twin-gyred structure make it indisputably a modon, at least for a short time.

The behavior of each of these two $|\alpha| = 45.0°$ cases can be contrasted with the observations of EXP 43. Unlike EXPs 40 and 27, no modon emerges because $2r_0$ is simply too large. Detailed observations of the motion of the barotropic vortex pair as well as the baroclinic rider and other modon quantities (Section 5) indicate that modongenesis did not occur.

The remaining large-α cases, $|\alpha| = 90.0°$ (EXPs 26, 38, 39), $\alpha = -135.0°$ (EXP 41), and $\alpha = 180.0°$ (EXPs 25, 42) differ only superficially and so may be discussed together. While we do not expect modongenesis on the basis of the early-time calculations in Section 3, only EXPs 25, 26 and 41 actually exhibit vortex separation (Fig. 12). In the configurations represented by EXPs 38 and 39, the eddies are sufficiently close together ($2r_0 = 0.67$ and 0.33) and properly aligned ($\alpha = -90.0°$, see Fig. 2) that the stronger (100 cm s^{-1} cyclonic) eastern vortex advects the weaker (25 cm s^{-1} anticyclonic) western vortex to the southeast. Having done so, their strengths then assure modongenesis even though subsequent oscillation (analogous to that in Figs. 9, 10 for EXP 40) complicates the picture. The significant fact, however, is that the scenario $\alpha = -90.0°$ can result in modongenesis. If the initial position of the vortices were reversed ($\alpha = +90.0°$), the more intense (cyclonic) eddy would advect the weaker (anticyclonic) vortex to the north ($\alpha = 180.0°$), and modongenesis would not be possible. Even more experiments than were done in this work would therefore probably reveal that the modongenesis boundary in Fig. 2 should

be indented toward the origin $(2r_0, \alpha) = (0, 0)$ as $\alpha \uparrow +90.0°$.

The sole remaining case, EXP 42, exhibits behavior that is rather unexpected. In Fig. 13, we show contours of constant P_{BT} for this $\alpha = 180.0°$ configuration. The stronger cyclonic vortex advects the weaker northern one to the west, thus augmenting its westward propagation tendency. By day 6, only the more vigorous barotropic vortex and superposed baroclinic part (not shown in this barotropic map) are present. The baroclinic vortex is now unstable to modongenesis by the nonlinear mechanism of McWilliams and Flierl (1979). Although the birth of the modon does not correspond to the more familiar $\alpha = 0.0°$ configuration, the interesting point is that the low pressure barotropic eddy is retained and a barotropic high emerges southeast of it.

These simulations not only reinforce many of the conclusions of Section 3, but also greatly expand and refine their scope. We have performed experiments in which the inclination angle and separation distance have been varied, and modongenesis has re-

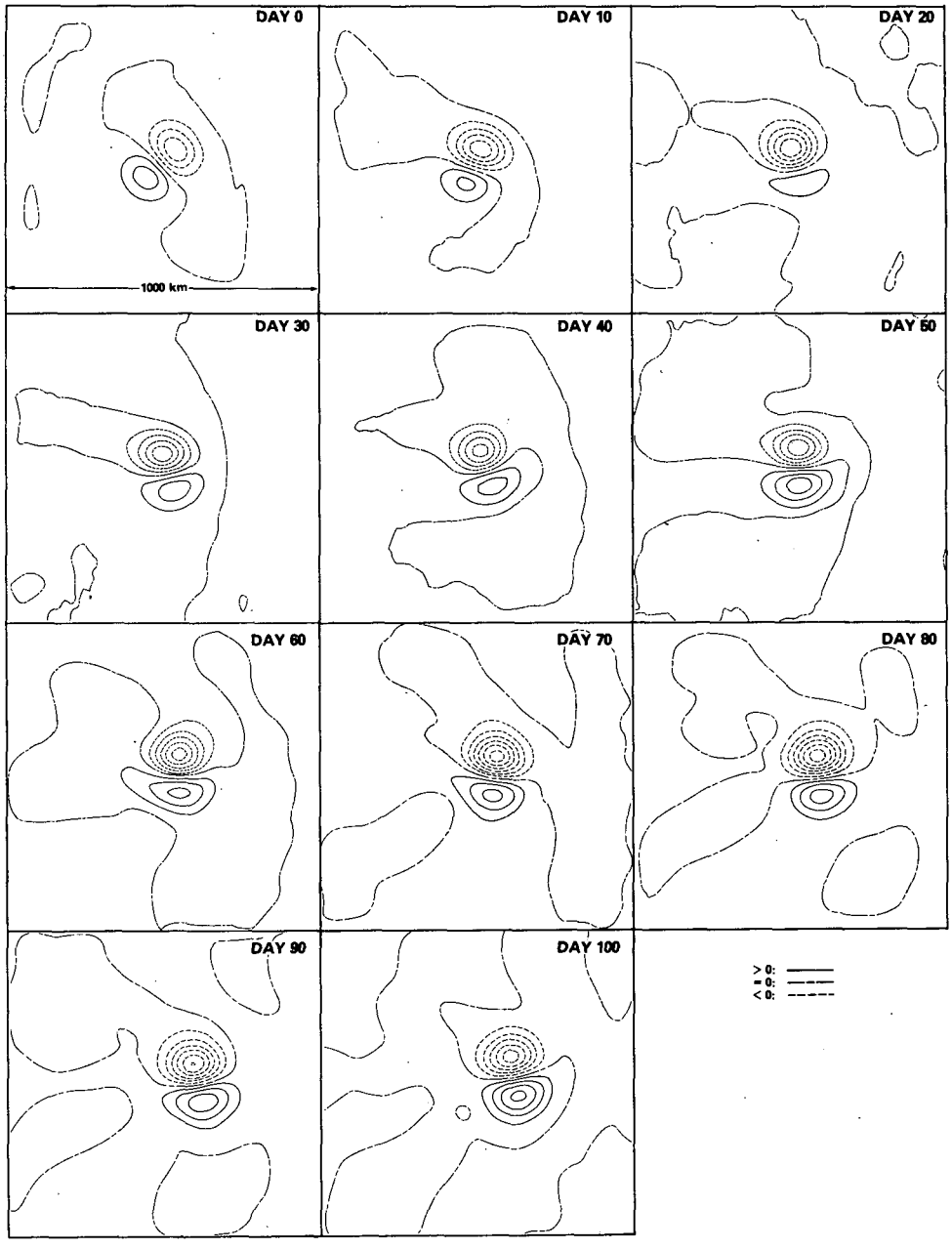

FIG. 10. Contours of P_{BT} for EXP 40 on day 0 and every tenth succeeding day. Contour code as in Fig. 4. Contour interval = 0.25 m^2 s^{-2}. The box is 1000 km square.

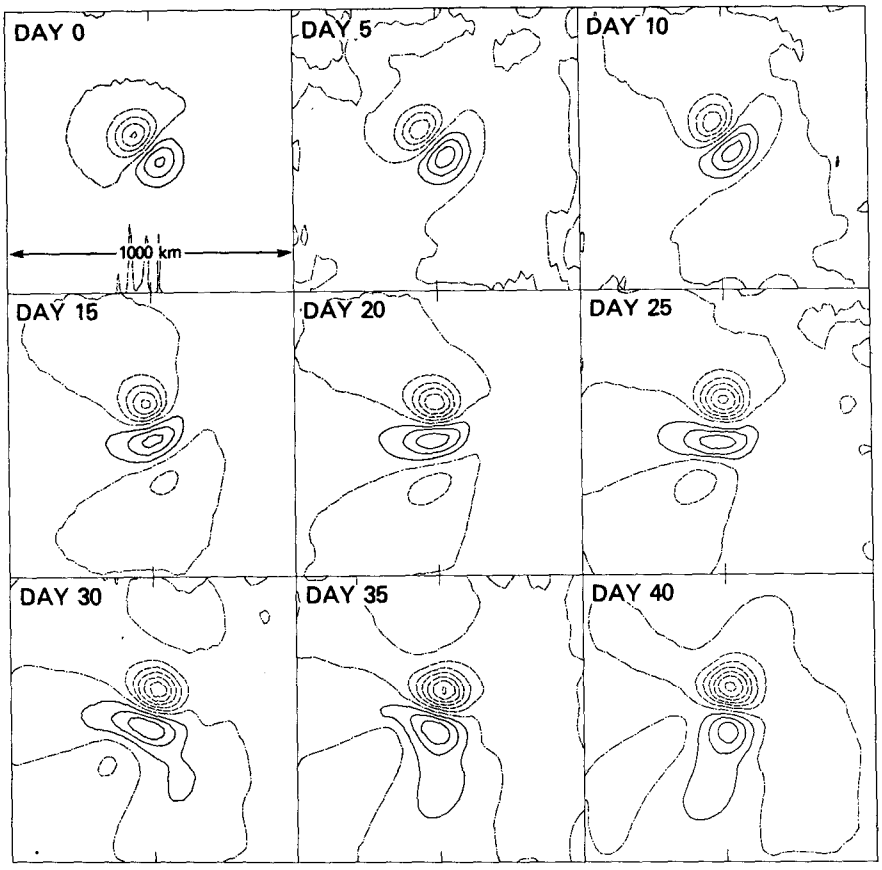

FIG. 11. P_{BT} contours of EXP 27 for days 0–40 in 5-day increments. Contour code as in Fig. 4, and contour interval = 0.3 $m^2 s^{-2}$. The box is 1000 km square.

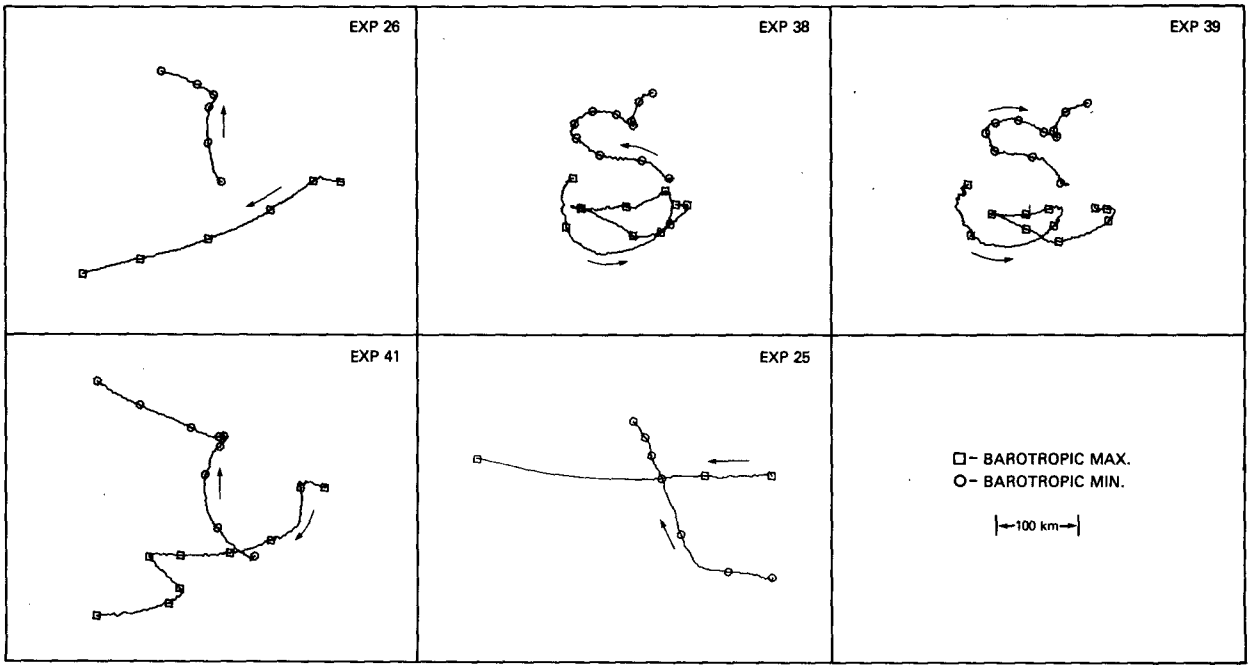

FIG. 12. Trajectory of the extrema in the barotropic pressure of EXPs 26, 38, 39, 41, and 25. Data points denote position at day 0 and every tenth day thereafter.

sulted in a surprisingly large number of these cases. In the next Section, we shall examine in detail how well these modons are described by the theory of Section 2.

5. Modon propagation

In this section, we examine the measured properties of the modons which result from EXPs 12, 21, 22, 27, 38, 39, 40 and 42. Of particular interest are the speeds, length scales, and magnitudes of these eastward-propagating current systems. Because the Larichev and Reznik core is the most essential part, more attention will be devoted to the barotropic flow properties than to those of the baroclinic flow.

In Section 4, we noted that some ambient noise is present in the experiments and that its barotropic component is larger than the baroclinic one. This

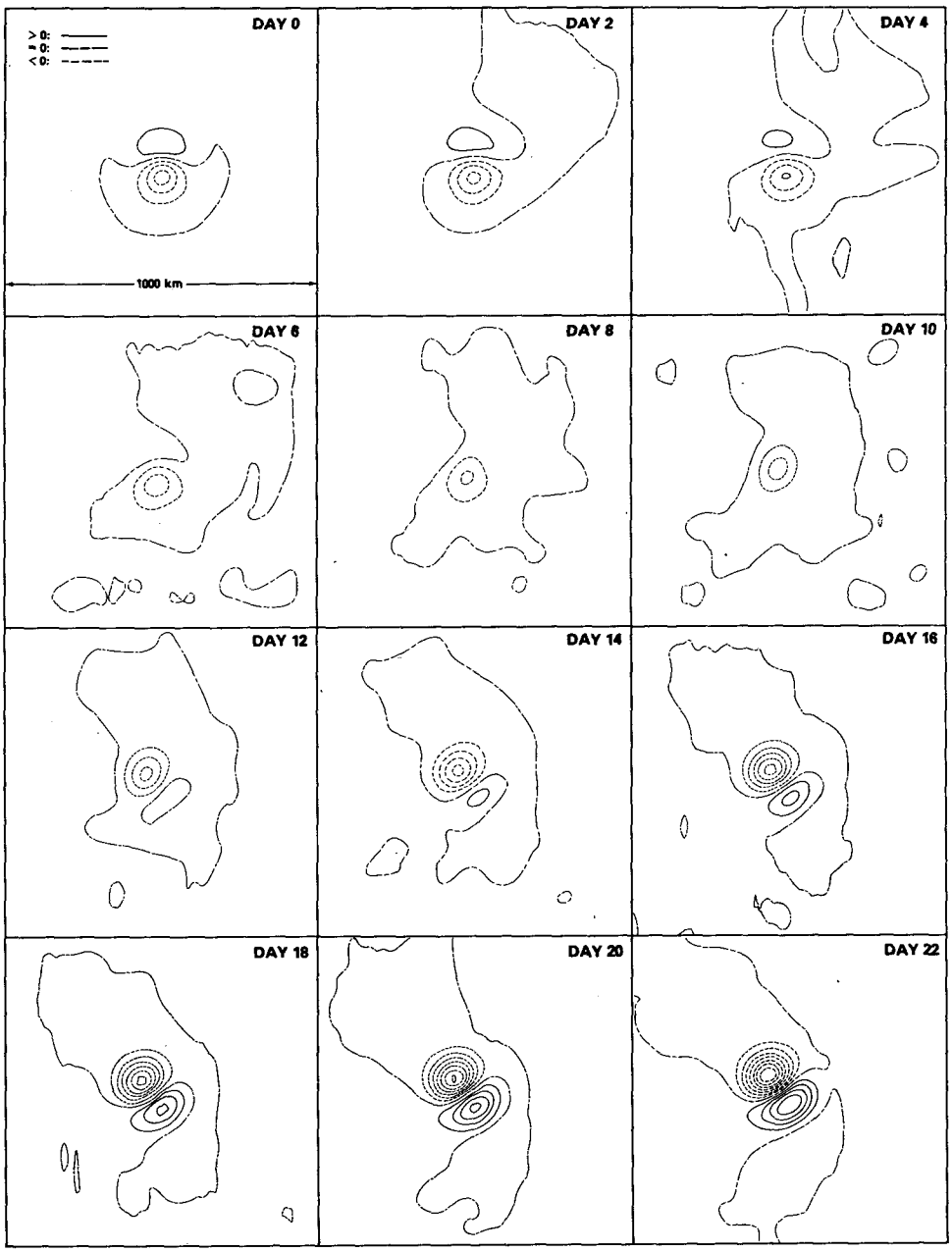

FIG. 13. P_{BT} contours of EXP 42 on day 0 and on each succeeding second day. Contour code as in Fig. 4. Contour interval = 0.125 $m^2 s^{-2}$. The computational box is 1000 km square.

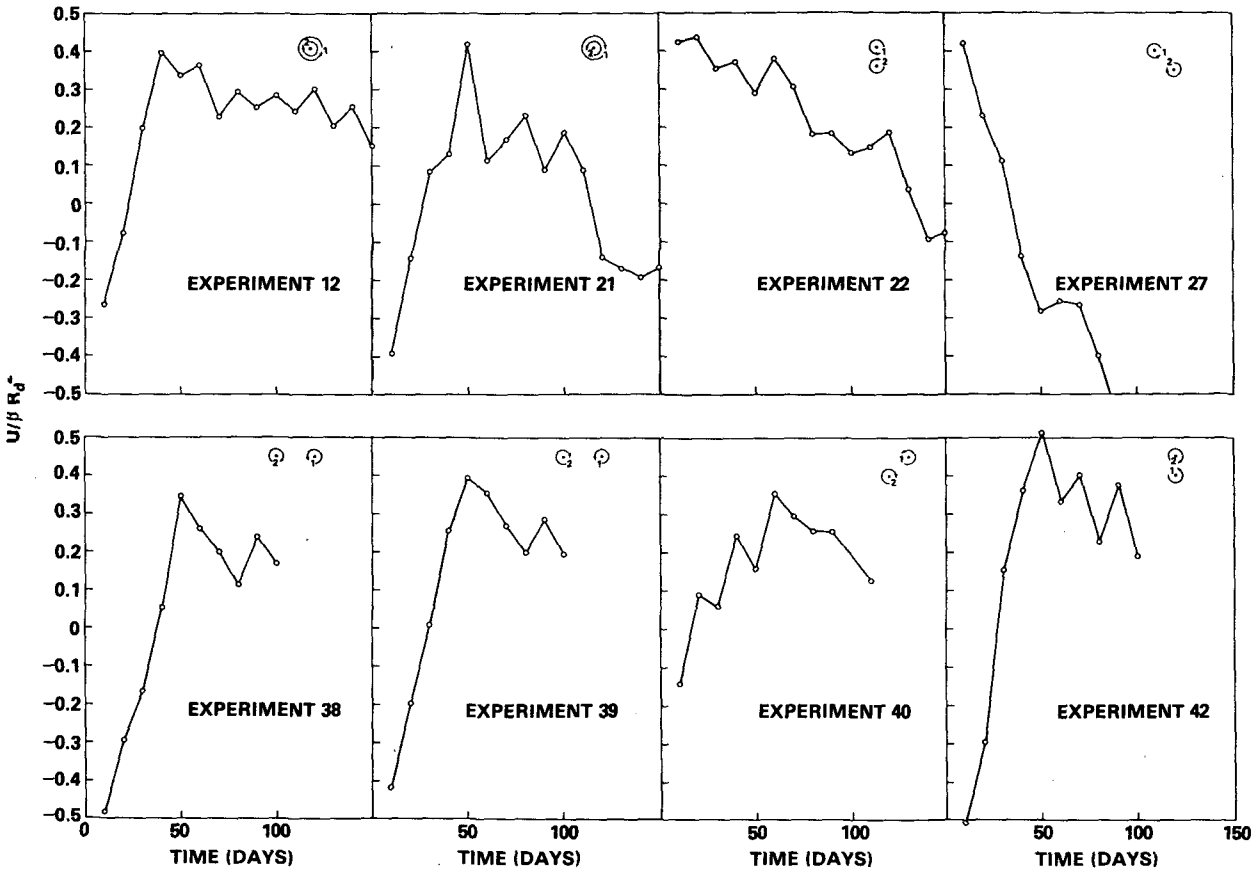

FIG. 14. A collage of the eastward ($+x$) speed records $U/\beta R_d^2$ of the modons in EXPs 12, 21, 22, 27, 38, 39, 40, and 42. The direction of flow in the upper (1) and lower layers (2) is shown, as are the relative angular positions of the initial eddy locations.

contaminates the speed data by advecting the modon with a time-dependent current and so masks the actual speed of the vortices. Moreover, the intensity of the modon (hence its speed) changes as it propagates. This is caused by its nonlinear evolution and the gradual energy dissipation by viscosity.

By measuring the speed of the attached baroclinic vortex over a ten day period centered on the day of interest, we can obtain a record of the fluctuating signal. These plots are shown in Fig. 14 and reveal a great deal about modon propagation. Although these speeds fluctuate a great deal, it is apparent from all of the curves that after modongenesis has occurred, there is a slow decrease in the eastward propagation speed. We expect this because, as viscosity acts to decrease the core pressure, the modon travels slower. It may happen that this decrease in strength destroys the nonlinear balance essential to the existence of a modon. When this happens (as in EXPs 21, 22, 27), the two vortices separate and propagate westward ($U/\beta R_d^2 < 0$) independently.

The question of strength[2] ($\max\psi_{BT}/\beta a^3$) required for a Larichev and Reznik (1976) modon with given gyre separation to propagate steadily eastward has been approached by Flierl *et al.* (1980). In the strictest sense, none of these simulations represent modons which propagate steadily eastward with unchanging magnitude. However, it is instructive to compare the observed parameters with the limitations placed upon them by the mathematical model. In Fig. 15, we show the position of the eight modons of this paper on Fig. 11 of Flierl *et al.* The cross-hatched area is merely the graphical representation of the information in Table 3. It represents the observed mean l_{BT}/a and $\max\psi_{BT}/\beta a^3$, as well as the uncertainties in their measurement. When the *average* lengths and barotropic core pressures from Table 3 are examined, we see that all but those of EXP 22 lie in the parameter range permitted by the analytical theory. Nevertheless, the observed parameters do venture out of the allowable area while the modon is actively evolving. The implication of Fig. 15 is therefore that the steady-state modon theory is only an approximate

[2] Because the baroclinic deformation radius R_d used to nondimensionalize the equation in Section 3 is meaningless in this barotropic context, the modon radius a is used.

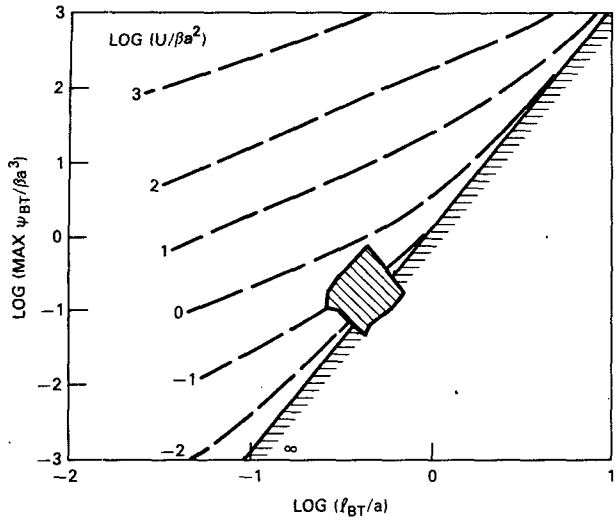

FIG. 15. $U/\beta a^2$ as a function of l/a (after Flierl *et al.*, 1980) on which the position of the modons and measurement uncertainties are shown. This information is contained in Table 3.

guide to what might be expected in an unsteady experiment.

Not only in the measurement of translation velocities does a fluctuation appear, but also in other measurable quantities as well. Table 3 shows speeds ($U/\beta R_d^2$), separation distances of the barotropic gyres in the modon core ($=2l_{BT}/R_d$ or $2l/a$ depending upon the nondimensionalization), the strength parameter of the modon core ($\max\psi_{BT}/\beta a^3$), the radius of maximum baroclinic current (l_{BC}/R_d) and the radius (a/R_d).

Fig. 16 shows the position of the modon parameters and their uncertainties on the baroclinic rider diagram of Flierl *et al.* (1980). Also shown is the dispersion relation for the continuous-vorticity baroclinic rider (Section 2). Along this curve, the quantity $\nabla^2\psi_{BC}$ is continuous across the line $r = a$. We remark however, the grouping of the experiments about this line does not necessarily imply that modons favor the $[\nabla^2\psi_{BC}]_{r=a} = 0$ configuration. Their proximity to this curve may simply be an artifact of the initial conditions. It is interesting to note, however, that locating the experiments with respect to $U/\beta R_d^2$ and a/Rd implies that $\psi_{BC}(r = a)/\psi_{BC}(r = 0) \geqslant 0$. Because a was calculated (rather than measured) from a knowledge of $U/\beta R_d^2$ and l_{BT}/R_d, it has a wide range of variation since measurements of the speed are very imprecise, as noted above. This indicates that measurements of $\psi_{BC}(r = a)/\psi_{BC}(r = 0)$ would be of concomitantly poor accuracy. Nevertheless, it is encouraging that the qualitative evaluation of all the baroclinic data for the eight modons reveal this ratio to be always positive, which would be consistent with the placement of the experiments on the graph.

By examining a north–south cut at the longitude about which the two barotropic vortices are centered, we may use a least-squares technique to fit the data with a pressure distribution appropriate to a barotropic modon and its barotropic rider (2.1). This process supplies κ and the true center of the barotropic core, from which l_{BT} may be calculated (Section 2). Knowing κ and U, we may use Eq. (2.4) to find the modon radius a. In Fig. 17, the results of

TABLE 3. The speed ($U/\beta R_d^2$), barotropic length scale (l_{BT}/R_d and l_{BT}/a), modon strength ($\max\psi_{BT}/\beta a^3$), radius of maximum baroclinic currents (l_{BC}/R_d) for the rider, and the radius (a/R_d) for the eight modongenesis experiments of the total of thirteen.

Experiment	$U/\beta R_d^2$	l_{BT}/R_d	l/a	$\frac{\max\psi_{BT}}{\beta a^3}$	l_{BC}/R_d	a/R_d
12	$0.270^{+0.129}_{-0.119}$	$1.129^{+0.296}_{-0.268}$	$0.438^{+0.285}_{-0.175}$	$0.156^{+0.253}_{-0.092}$	$1.235^{+0.216}_{-0.098}$	$2.578^{+0.692}_{-0.606}$
21	$0.168^{+0.252}_{-0.083}$	$1.628^{+0.088}_{-0.085}$	$0.414^{+0.041}_{-0.029}$	$0.057^{+0.014}_{-0.014}$	$1.191^{+0.139}_{-0.047}$	$3.930^{+0.075}_{-0.159}$
22	$0.264^{+0.175}_{-0.227}$	$1.354^{+0.249}_{-0.237}$	$0.429^{+0.156}_{-0.128}$	$0.096^{+0.107}_{-0.054}$	$1.193^{+0.145}_{-0.106}$	$3.159^{+0.553}_{-0.421}$
27	$0.253^{+0.166}_{-0.144}$	$1.014^{+0.154}_{-0.214}$	$0.442^{+0.188}_{-0.136}$	$0.256^{+0.412}_{-0.111}$	$1.225^{+0.091}_{-0.100}$	$2.296^{+0.318}_{-0.451}$
38	$0.198^{+0.149}_{-0.145}$	$1.202^{+0.312}_{-0.220}$	$0.428^{+0.208}_{-0.150}$	$0.156^{+0.217}_{-0.130}$	$1.184^{+0.159}_{-0.102}$	$2.809^{+0.727}_{-0.427}$
39	$0.280^{+0.115}_{-0.083}$	$1.202^{+0.243}_{-0.211}$	$0.435^{+0.201}_{-0.137}$	$0.147^{+0.261}_{-0.114}$	$1.253^{+0.111}_{-0.087}$	$2.761^{+0.563}_{-0.490}$
40	$0.204^{+0.151}_{-0.144}$	$1.219^{+0.251}_{-0.246}$	$0.428^{+0.198}_{-0.143}$	$0.116^{+0.169}_{-0.069}$	$1.252^{+0.164}_{-0.112}$	$2.849^{0.564}_{-0.500}$
42	$0.320^{+0.194}_{-0.167}$	$1.214^{+0.318}_{-0.217}$	$0.439^{+0.221}_{-0.153}$	$0.168^{+0.245}_{-0.127}$	$1.186^{+0.070}_{-0.102}$	$2.768^{+0.724}_{-0.446}$

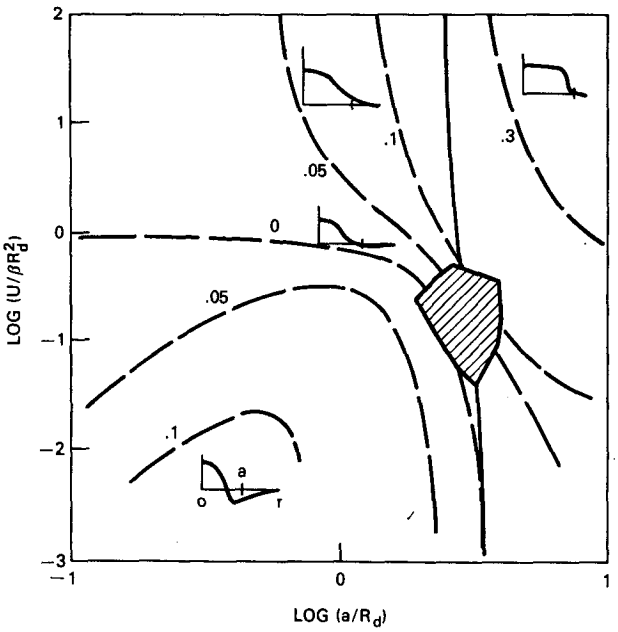

FIG. 16. Plot of modon speed as a function of radius (after Flierl *et al.*, 1980) from Table 3. The dashed lines are levels of $\psi_{BC}(r = a)/\psi_{BC}(r = 0)$ and the dispersion relation with the restriction $[\nabla^2\psi_{BC}]_{r=a} = 0$ is shown as a solid line. The four small graphs show the rider pressure as a function of radius.

treating the barotropic data in this fashion are exhibited and thus some general conclusions may be drawn. The modons of EXPs 12, 21, 22, and 42 arise from the nonlinear process of McWilliams and Flierl (1979), or from initial conditions proximate to those of a modon state. As such, these experiments exhibit vortex trajectories which are much less complicated than those of the other modon experiments. Their core and rider pressures exhibit fairly distinct trends. After the initial evolution period, there is a slow decrease in the mean core pressure (after fluctuations are visually averaged out). This is due to the dissipative action of viscosity upon the modon.

On the other hand, instances of modongenesis when $|\alpha| \geq 45.0°$ are generally associated with large angular swings of the line of centers of the two vortices (EXPs 27, 38, 39, and 40) as the modon evolves to a nearly-steady state. This makes core and rider pressures very unsteady as derived. The persistence of these vortex pairs as identifiable, eastward-propagating modons is therefore all the more remarkable. It suggests that these current systems may be even more stable than previously thought (McWilliams *et al.*, 1981).

6. Conclusion

The question to which we have addressed ourselves is whether a modon can result from an eddy with a tilted vertical axis and counter-rotating upper and lower-ocean gyres. We have modeled this scenario by placing a vortex in each layer of a two-layer ocean and separating their centers by many tens of kilometers. Simple modal decomposition then reveals that the initial barotropic flow consists of a vortex pair which at least superficially resembles the modon described by Larichev and Reznik. The positioning of this vortex pair constitutes an initial value problem

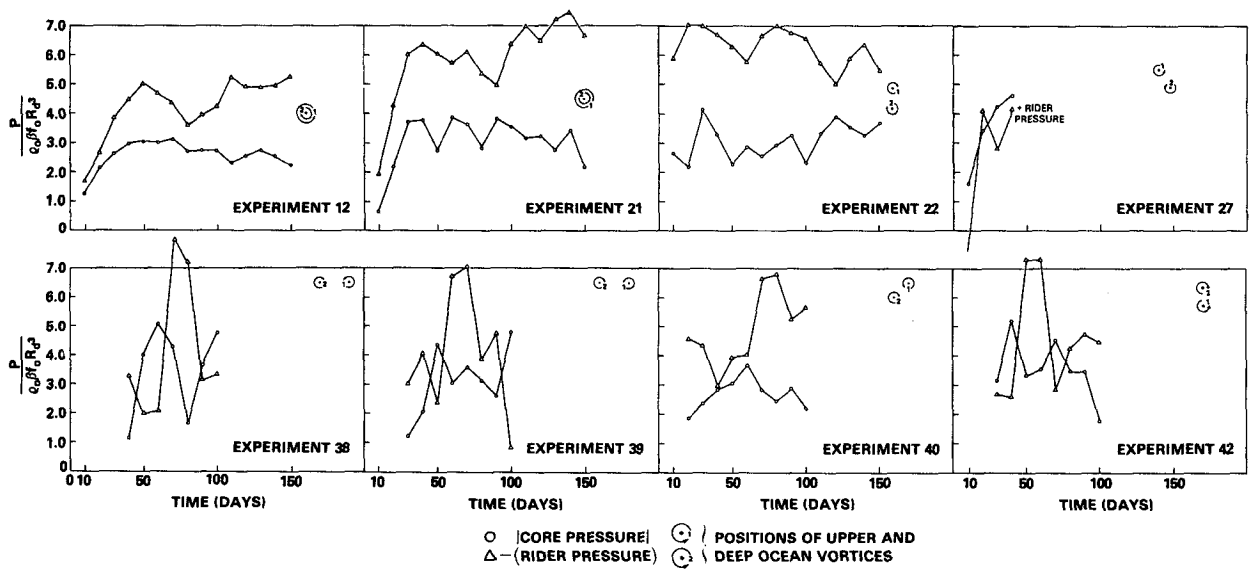

FIG. 17. The modon core pressure and that of the barotropic riders for EXPs 12, 21, 22, 27, 38, 39, 40, and 42. The short-lived EXP 27 modon possesses an anticyclonic rider (pressure > 0). The direction of rotation in the upper (1) and lower layers (2) is shown, as are the relative angular positions of the initial eddy locations.

which leads to either modongenesis or physical separation of the two vortices.

In cases where modongenesis ensues, the flow is found to consist of the Larichev and Reznik, (1976) core and attached barotropic and baroclinic vortices (Stern, 1975; Flierl *et al.*, 1980). Since these two types of riders do not alter the dynamics of the core (and in fact, cannot exist without it), we concentrate on the evolution of the barotropic flow, at least for early time. A small-time expansion has been used on the barotropic quasigeostrophic equation and the resulting Poisson equation solved by Fourier transforms to indicate the initial motion of the two vortices. We find that the barotropic solution to $O(t)$ is determined by the propagation/dispersion and mutal advection tendencies. When Gaussian vortices with radial velocities proportional to $re^{-r^2/2L^2}$ are used in each layer, we find that modongenesis is indicated when the separation distance is $\leqslant(1.5\text{–}2.0)\ L$ and their line of centers with the cyclonic vortex to the north is aligned along $\alpha = 0.0°$. As $|\alpha| \uparrow 90.0°$, the minimum separation distance required for modongenesis decreases to zero. The actual numerical calculations, however, reveal that any tilted axis baroclinic eddy *of sufficient strength* will probably evolve into a modon (regardless of the value of α) if only the separation distance is $\leqslant L/3$ ($\sim$20 km in this work). The mechanisms which bring this about are either a nonlinear evolution, or the bodily advection of one vortex by the other, until the $\alpha \approx 0.0°$ configuration is reached.

The numerical experiments are of 100–150 days duration so that the temporal behavior of all modon parameters can be compared with those of the inviscid, quasigeostrophic model. We find that the speeds and barotropic vortex separation (Fig. 15) are in the permissible propagation region in seven of the eight cases for modons of this type. Although a sufficiently precise determination of modon radius could not be made, location of the modons on a $U/\beta R_d^2$ vs a/R_d graph (Fig. 16) indicates that $P_{BC}(r = a)/P_{BC}(r = 0) > 0$ for all modons, which is in qualitative agreement with the experimental findings.

In their modon experiments, McWilliams *et al.* (1981) observe an amplitude decay and concomitant decrease in zonal speed. Although we see a decrease in eastward propagation speed (Fig. 14), the continuing evolution of the modon core and barotropic rider (Fig. 17) render similar conclusions on amplitude in this work difficult. Although we see instances of core pressure decay, it is sometimes observed to increase slightly as energy is interchanged with the riders. Thus, any firm conclusions are ill-advised in these evolutionary experiments.

The success of many of these experiments in generating modons from quite unexpected configurations is striking. Even the most adverse scenarios (e.g. $\alpha = 180.0°$, EXP 42) have resulted in modongenesis provided the upper and deep ocean vortices are sufficiently strong and are less than $\sim$20 km apart. The willingness of tilted-axis baroclinic eddies to evolve into modons, as well as their sometimes complicated trajectories during evolution, suggests that they are not terribly fragile and may be even more durable than currently believed.

Unfortunately, unambiguous identification of these flows in the ocean is a significant problem, because the presence of the barotropic core can be totally masked by the baroclinic and barotropic riders.

Acknowledgments. The authors wish to thank Dr. J. A. DeSanto (NRL) for a helpful discussion on the early-time behavior of the eddies. We are especially grateful to Prof. G. R. Flierl (MIT) for allowing our use of Figs. 15 and 16, and for providing a pre-publication copy of the paper by Flierl *et al.* (1980).

REFERENCES

Abromowitz, M., and I. Stegun, 1965: *Handbook of Mathematical Functions*. Dover, 1046 pp.

Adem, J., 1956: A series solution for the barotropic vorticity equation and its application in the study of atmospheric vortices. *Tellus*, **8**, 3, 364–372.

Erdélyi, A., 1954: *Tables of Integral Transforms*, Vol. 1. McGraw-Hill, 398 pp.

Flierl, G. R., 1976: Contributions to the theory and modelling of eddies. *Theory and Modelling of Ocean Eddies: Contribution of the U.S. Delegation to the Yalta Polymode Theoretical Institute*, P. B. Rhines, Ed., 23 pp.

——, 1978: Models of vertical structure and the calibration of two-layer models. *Dyn. Atmos. Oceans*, **2**, 341–381.

——, V. D. Larichev, J. C. McWilliams and G. M. Reznik, 1980: The dynamics of baroclinic and barotropic solitary eddies. *Dyn. Atmos. Oceans*, **5**, 1–41.

Holland, W. R., and L. B. Lin, 1975: On the generation of mesoscale eddies and their contribution to the oceanic general circulation. I. A preliminary numerical experiment. *J. Phys. Oceanogr.*, **5**, 642–657.

Larichev, V. D., and G. M. Reznik, 1976: Two-dimensional Rossby soliton: an exact solution. *Polymode News*, No. 19, 3 and 6.

McCartney, M. S., L. V. Worthington and W. J. Schmitz, Jr., 1978: Large cyclonic rings from the northeast Sargasso Sea. *J. Geophys. Res.*, **83**, 901–914.

McWilliams, J. C., and G. R. Flierl, 1979: On the evolution of isolated, nonlinear vortices. *J. Phys. Oceanogr.*, **9**, 1155–1182.

——, G. R. Flierl, V. D. Larichev and G. M. Reznik, 1981: Numerical studies of barotropic modons. *Dyn. Atmos. Oceans*, **5**, 219–238.

Mied, R. P., and G. J. Lindemann, 1979: The propagation and evolution of cyclonic Gulf Stream rings. *J. Phys. Oceanogr.*, **9**, 1183–1206.

Savchenko, V. G., W. J. Emery and O. A. Vladimirov, 1978: A cyclonic eddy in the Antarctic Circumpolar current South of Australia: results of Soviet-American observations aboard the R/V *Profesor Zubov*. *J. Phys. Oceanogr.*, **8**, 825–837.

Stern, M., 1975: Minimal properties of planetary eddies. *J. Mar. Res.*, **33**, 1–13.